

---

# Discrete Langevin Sampler via Wasserstein Gradient Flow

---

**Haoran Sun**  
Georgia Institute of Technology  
hsun349@gatech.edu

**Hanjun Dai**  
Google Brain  
hadai@google.com

**Bo Dai**  
Google Brain  
bodai@google.com

**Haomin Zhou**  
Georgia Institute of Technology  
hmzhou@math.gatech.edu

**Dale Schuurmans**  
Google Brain & University of Alberta  
schuurmans@google.com

## Abstract

Recently, a family of locally balanced (LB) samplers has demonstrated excellent performance at sampling and learning energy-based models (EBMs) in discrete spaces. However, the theoretical understanding of this success is limited. In this work, we show how LB functions give rise to LB dynamics corresponding to Wasserstein gradient flow in a discrete space. From first principles, previous LB samplers can then be seen as discretizations of the LB dynamics with respect to Hamming distance. Based on this observation, we propose a new algorithm, the *Locally Balanced Jump* (LBJ), by discretizing the LB dynamics with respect to simulation time. As a result, LBJ has a location-dependent "velocity" that allows it to make proposals with larger distances. Additionally, LBJ decouples each dimension into independent sub-processes, enabling convenient parallel implementation. We demonstrate the advantages of LBJ for sampling and learning in various binary and categorical distributions.

## 1 Introduction

The Markov Chain Monte Carlo (MCMC) algorithm is one of the most widely used methods for sampling from intractable distributions (Robert & Casella, 2013). However, it also notoriously mixes slowly in complex, high-dimensional models. The past decades have witnessed the development of several gradient based MCMC methods that leverage gradient information to guide proposals toward high probability regions (Ma et al., 2015). By simulating Langevin dynamics, the Metropolis Adjusted Langevin Algorithm (Rossky et al., 1978) and its variants (Welling & Teh, 2011; Girolami & Calderhead, 2011) substantially improve sampling efficiency in both theory and practice. In a seminal work, Jordan et al. (1998) show that the Fokker-Planck equation associated with Langevin dynamics yields the Wasserstein gradient flow with respect to KL-divergence. This connection not only explains the excellent performance of Langevin algorithms, but it also provides a tool for algorithm design (Liu et al., 2019) and theoretical analysis (Cheng & Bartlett, 2018).

Despite many advances, progress in gradient based methods has generally focused on continuous spaces. Recently, a family of locally balanced (LB) samplers (Zanella, 2020; Grathwohl et al., 2021; Sun et al., 2021a) have leveraged gradient information for energy based models (EBMs) in discrete spaces, achieving significant success. Although Zanella (2020); Sun et al. (2021a) showed that LB functions are asymptotically optimal, a theoretical explanation of the good performance of LB samplers in finite dimensional problems remains lacking. Moreover, current LB samplers do not utilize the geometry associated with the target distribution. From Zanella (2020); Grathwohl et al. (2021), where one site is flipped per M-H step, to Sun et al. (2021a), where multiple sites are flipped

per M-H step via auxiliary paths, existing LB samplers for discrete spaces restrict the scale of the proposals to a given Hamming distance. Imposing a uniform change rate across all states reduces sampler efficiency. For example, imagine two high probability regions  $A, B$  connected through a low probability region  $C$ . If a sampler can use twice the change rate in  $C$ , then it can use half as many steps to transit from  $A$  to  $B$  through  $C$ , resulting in half the holding time in  $A, B$ , improving mixing.

To address the questions above, we lift the view of the sampling task to the distribution level. Here one can observe that distributions on a discrete space  $V$  form a manifold  $\mathcal{P}_2(V)$  Do Carmo & Flaherty Francis (1992), upon which we can define Riemannian metrics via optimal transport Villani (2009); Chow et al. (2012). In this paper, we show that the family of LB functions provides a systematic approach to designing LB dynamics  $X(t)$  that correspond to the Wasserstein gradient flow toward a target distribution  $\pi$ . Unsurprisingly, previous LB samplers can be seen as different discretizations of the LB dynamics, which explains their good performance in finite dimensional problems. Similar to the continuous case, the dynamics perspective also helps design new algorithms. Here we propose a novel sampler, the *locally balanced jump* (LBJ), by using a more efficient discretization of the LB dynamics. In particular, we factorize  $X(t)$  into sub-processes  $X^d(t)$ , where for each sub-process, we estimate the transition  $P^d(\tau)$  after a simulation time  $\tau$  and propose a new state according to  $P^d(\tau)$ . In this way, LBJ is (i) statistically more efficient since it uses a location dependent change rate that allows the proposal to make larger changes, and (ii) computationally more efficient as it decouples dimension and permits convenient parallel implementation.

An experimental evaluation demonstrates that LBJ enjoys better proposal quality and greater efficiency compared to traditional samplers and other LB samplers. We demonstrate advantages both in sampling and learning tasks involving binary and categorical distributions, including the Bernoulli distribution, Ising model, factorial hidden Markov model, restricted Boltzmann machine, and deep EBMs.

## 2 Preliminaries

**Metropolis-Hastings Algorithm.** Let  $\pi$  denote the target distribution. Given a current state  $x^{(n)}$ , a M-H sampler draws a candidate state  $y$  from a proposal distribution  $q(x^{(n)}, y)$ . Then, with probability  $\min\{1, \frac{\pi(y)q(y, x^{(n)})}{\pi(x^{(n)})q(x^{(n)}, y)}\}$  the proposed state is accepted and  $x^{(n+1)} = y$ ; otherwise it is rejected and  $x^{(n+1)} = x^{(n)}$ . In this way, the detailed balance condition is satisfied and the M-H sampler generates a Markov chain  $x_0, x_1, \dots$  that has  $\pi$  as its stationary distribution.

**Locally Balanced Function.** The locally balanced sampler is a class of M-H algorithms in discrete spaces. It uses proposal distributions  $q(x, y) \propto g(\pi(y)/\pi(x))$  for  $y$  in the neighborhood of  $x$  (e.g. 1-Hamming ball). The weight function  $g$  satisfies  $g(t) = tg(\frac{1}{t})$  and is called the locally balanced function. Two commonly used locally balanced functions are  $g(t) = \sqrt{t}$  and  $g(t) = \frac{t}{t+1}$ . Zanella (2020) and Sun et al. (2021a) prove that a locally balanced function is asymptotically optimal for single-step and multi-step proposals, respectively.

**Langevin Dynamics.** The Langevin dynamics  $dx = f(x)dt + \sqrt{2}dW_t$  specify a stochastic differential equation describing the movement of a particle under the influence of drag and random forces. The time evolution of the probability density function is determined by a partial differential equation:  $\frac{\partial}{\partial t}\rho(x, t) = -\frac{\partial}{\partial x}[f(x)\rho(x, t)] + \frac{\partial^2}{\partial x^2}\rho(x, t)$ , which is called the Fokker-Planck equation.

**Otto Calculus.** The Wasserstein space  $\mathcal{P}_2(\mathbb{R}^d)$  is a manifold over probability measures on  $\mathbb{R}^d$  such that the shortest distance between two measures  $\mu, \nu$  in the manifold is exactly the Wasserstein distance between  $\mu$  and  $\nu$  (Villani, 2009). Given a target distribution  $\pi \in \mathcal{P}_2(\mathbb{R}^d)$ , where  $\pi(x) \propto e^{-f(x)}$ , the gradient flow in terms of the KL-divergence  $D_{\text{KL}}(\rho||\pi)$  is given by the Fokker-Planck equation above (Jordan et al., 1998).

## 3 Wasserstein Gradient Flow for Discrete Distributions

Given a finite set  $V = \{1, \dots, M\}$ , the distributions over  $V$  form a manifold  $\mathcal{P}(V) = \{\rho \in \mathbb{R}^M : \sum_{i=1}^M \rho_i = 1, \rho_i \geq 0\}$  with tangent space  $T_\rho \mathcal{P}(V) = \{\sigma \in \mathbb{R}^M : \sum_{i=1}^M \sigma_i = 0\}$  (Do Carmo & Flaherty Francis, 1992). We want to sample from the target distribution  $\pi_i \propto \exp(-f_i)$ , where  $f$  is an energy function. Given an initial distribution  $\rho^0$ , a natural way to find a path from  $\rho^0$  to the target distribution  $\pi$  is to perform gradient descent in the KL-divergence  $D_{\text{KL}}(\rho||\pi)$ . In this section, we will first show that how to properly design the Wasserstein distance on  $\mathcal{P}(V)$ . Then, we derive the

gradient flow on the manifold with respect to the Wasserstein metric. Finally, we show that locally balanced functions naturally induce dynamics that simulate the gradient flow, allowing a tractable particle level sampling algorithm.

### 3.1 Wasserstein Metrics on Graphs

Metropolis-Hastings (M-H) algorithms in discrete spaces typically restrict the support of the proposal distributions to lie within the neighborhood  $N(i)$  of the current state  $i$ , due to computational concerns. To obtain gradient flows that can be simulated in practice, we introduce a neighborhood structure  $N(\cdot)$  to  $V$  by considering the graph  $G = (V, E)$ , where  $(i, j) \in E$  if  $j \in N(i)$ . In this case, we can first design the Wasserstein distance on  $G$  then use it to induce metrics on  $\mathcal{P}(V)$ . Without loss of generality, assume  $G$  is connected. On every edge  $(i, j)$ , we assign a weight  $g_{ij}(\rho) = g_{ij}(\rho) > 0$  depending on the current position  $\rho \in \mathcal{P}(V)$ . Following Chow et al. (2012, 2017), define the vector field on  $G$  as a matrix  $v = (v_{ij})_{i,j=1}^M$  such that  $v_{ij} = -v_{ji}$  and  $v_{ij} = 0$  if  $(i, j) \notin E$ . Then on the graph  $G$ , the divergence of a vector field is:

$$\operatorname{div}_\rho(v) := -\left(\sum_{j \in N(i)} g_{ij}(\rho)v_{ij}\right)_{i=1}^M \in T_\rho\mathcal{P}(V) \quad (1)$$

and the inner-product of two vector fields is:

$$\langle u, v \rangle_\rho := \frac{1}{2} \sum_{(i,j) \in E} g_{ij}(\rho)u_{ij}v_{ij} \quad (2)$$

We introduce the coefficient  $\frac{1}{2}$  since every edge is included in  $E$  twice as  $(i, j)$  and  $(j, i)$ . With the inner-product, the 2-Wasserstein distance between two distributions  $\rho^0, \rho^1$  on  $G$  can be established via the Benamou-Brenier formula Benamou & Brenier (2000):

$$W_2(\rho^0, \rho^1) := \inf_v \left\{ \left( \int_0^1 \langle v^t, v^t \rangle_\rho dt \right)^{\frac{1}{2}} : \frac{d\rho^t}{dt} = \operatorname{div}_\rho(v^t) \right\} \quad (3)$$

The metrics on  $T_\rho\mathcal{P}(V)$  associated with  $W_2$  can be determined via the following two lemmas.

**Lemma 3.1.** *For any  $\rho \in \mathcal{P}(V)$  and any vector field  $u$ , the minimizer  $v^* = \arg \min_v \langle v, u \rangle$ , subject to  $\operatorname{div}_\rho(v) = \operatorname{div}_\rho(u)$ , is a potential field  $\nabla\Phi$ . That is, there exists a function  $\Phi : V \rightarrow \mathbb{R}$ , such that  $v_{ij}^* = \nabla\Phi_{ij} = (\Phi_i - \Phi_j)1_{\{(i,j) \in E\}}$ .*

We note that a potential field is invariant up to a constant shift, meaning that if  $\Phi$  is a potential function and  $\Phi' = \Phi + c = (\Phi_i + c)_{i=1}^M$ , then  $\nabla\Phi' = \nabla\Phi$ . Hence, we consider an equivalence class  $[\Phi] = \{\Phi' \in \mathbb{R}^M : \exists c \in \mathbb{R}, \Phi' = \Phi + c\}$  and denote  $P^M = \{[\Phi] : \Phi \in \mathbb{R}^M\}$

**Lemma 3.2.** *For any  $\rho \in \mathcal{P}(V)$ , the mapping  $\zeta([\Phi]) = \operatorname{div}_\rho(\nabla\Phi)$  is a linear isomorphism between the set of equivalence classes  $P^M$  and the tangent space  $T_\rho\mathcal{P}(V)$ .*

The isomorphism  $\zeta$  induces a metric on the tangent space  $T_\rho\mathcal{P}(V)$ :

**Definition 3.3.** For any  $\rho \in \mathcal{P}(V)$ , we define the inner-product  $\langle \cdot, \cdot \rangle_\rho$  on  $T_\rho\mathcal{P}(V)$  as follows. Denote  $\Phi^\sigma \in \zeta^{-1}(\sigma)$ . Then for arbitrary  $\sigma^1, \sigma^2 \in T_\rho\mathcal{P}(V)$ , define

$$\langle \sigma^1, \sigma^2 \rangle_\rho = \sum_{i=1}^M \sigma_i^1 \Phi_i \sigma_i^2 \quad (4)$$

We denote the Riemannian manifold equipped with the metric (4) as  $\mathcal{P}_2(V)$ . The next corollary shows that  $\mathcal{P}_2(V)$  is a Wasserstein space.

**Corollary 3.4.** *On  $\mathcal{P}_2(V)$ , the distance between two distributions  $\rho^0, \rho^1$  can be written as:*

$$W_2(\rho^0, \rho^1) := \inf_v \left\{ \left( \int_0^1 \langle \sigma^t, \sigma^t \rangle_\rho dt \right)^{\frac{1}{2}} : \frac{d\rho^t}{dt} = \sigma^t \right\} \quad (5)$$

### 3.2 Locally Balanced Dynamics

In Otto's calculus, the gradient flow on Wasserstein space  $\mathcal{P}_2(\mathbb{R}^d)$  is given by the Fokker-Planck equation. Similarly, we characterize the gradient flow on  $\mathcal{P}_2(V)$ :

**Theorem 3.5.** *On the Riemannian manifold  $\mathcal{P}_2(V)$ , the gradient flow of  $D_{KL}(\rho||\pi)$  is:*

$$\frac{d}{dt}\rho_i = \sum_{j \in N(i)} g_{ij}(\rho)(f_j + \log \rho_j - f_i - \log \rho_i) \quad (6)$$

Equation (6) can be interpreted as a special case of the generic Fokker-Planck equation in a discrete space (Chow et al., 2012). Unfortunately, a practical algorithm to solve the Fokker-Planck equation in discrete spaces is not available, to the best of our knowledge. At the distribution level, the state space  $V$  is usually exponentially large, so directly solving the ODE for  $\rho$  at the distribution level is intractable. At the particle level, a simulation requires knowledge of the current distribution  $\rho$ , for example the  $\log \rho$  on the right hand side of (6), which is also intractable.

Although a solution for the generic Fokker-Planck equation is not known, we find, surprisingly, that locally balanced functions provide a simple but effective approach for simulating the Wasserstein gradient flow (6). In particular, for an arbitrary locally balanced function  $g$ , consider the logarithmic mean as the edge weight for edge  $(i, j) \in E$ :

$$g_{ij}(\rho) = \frac{g(\pi_i/\pi_j)\rho_j - g(\pi_j/\pi_i)\rho_i}{\log(g(\pi_i/\pi_j)\rho_j) - \log(g(\pi_j/\pi_i)\rho_i)} = \frac{g(\pi_i/\pi_j)\rho_j - g(\pi_j/\pi_i)\rho_i}{f_j + \log \rho_j - f_i - \log \rho_i} \quad (7)$$

By substituting the edge weight  $g_{ij}$  into the gradient flow (6), the intractable term  $\log \rho$  is cancelled and we obtain the following locally balanced gradient flow:

$$\frac{d}{dt}\rho^t = \rho^t Q, \quad Q_{ij} = \begin{cases} g(\pi_i/\pi_j), & j \in N(i) \\ -\sum_{k \in N(i)} Q_{ik}, & j = i \\ 0, & \text{else} \end{cases} \quad (8)$$

which is a Markov jump process that converges to the target distribution  $\pi$  exponentially fast. We name the corresponding dynamics as *locally balanced dynamics*, which can be described as a differential equation with respect to the transition probability:

$$\frac{d}{dh}\mathbb{P}(X(t+h) = j | x(t) = i) = g\left(\frac{\pi_j}{\pi_i}\right)1_{\{j \in N(i)\}} \quad (9)$$

## 4 Simulating the Locally Balanced Dynamics

Next, we study LB samplers for discrete spaces of the form  $V = \mathcal{X}^D$  where  $\mathcal{X} = \{e_1, \dots, e_n\}$  is a finite set of one-hot vectors. We assume the energy function  $f$  is differentiable and the neighborhood  $N(\cdot)$  is the 1-Hamming ball. Similar to gradient based M-H algorithms that simulate Langevin dynamics, we can design various locally balanced samplers for such a space by simulating (9). For example, the Gillespie algorithm Gillespie (1977) can simulate a continuous-time trajectory exactly satisfying the target distribution  $\pi$ . Here, we only care about the distribution behind the trajectory, so we will focus on efficient simulations of the Markov chain.

### 4.1 Casting Previous Locally Balanced Samplers as Locally Balanced Dynamics

We first show that previous locally balanced samplers are essentially using different discretizations of the locally balanced dynamics (9). The approximation error of  $\langle \nabla f(x), y - x \rangle$  for  $f(y) - f(x)$  is repaired by the M-H test and we ignore such differences in this section.

**Single Jump:** Denote the current state as  $x$ . LB-1 (Zanella, 2020) and GWG (Grathwohl et al., 2021) propose a new state  $y \in N(x)$  with probability  $q(x, y) \propto g(\pi_y/\pi_x)$  and  $q(x, y) \propto g(\exp(-\langle \nabla f(x), y - x \rangle))$ , respectively. In (9), the jump from  $x$  to  $y \in N(x)$  occurs at time  $\tau_y \sim \text{exponential}(g(\pi_y/\pi_x))$ . Then, by the property of the exponential distribution,  $\mathbb{P}(\arg \min_z \tau_z = y) \propto g(\pi_y/\pi_x)$ , the probability of the first jump satisfies the same multinomial distribution. Hence, one can state that LB and GWG propose the new state by simulating at which dimension the jump of the locally balanced dynamics occurs.

**Multiple Jumps:** Denote the current state as  $x = \sigma^0$  and the given path length as  $L$ . PAFS (Sun et al., 2021a) proposes a new state  $\sigma^L$  along the auxiliary path  $\sigma$ , where PAFS sequentially proposes  $q(\sigma^{l-1}, \sigma^l) \propto g(\exp(-\langle \nabla f(\sigma^0), \sigma^l - \sigma^{l-1} \rangle))$  for  $\sigma^l \in N(\sigma^{l-1})$ ,  $l = 1, \dots, L$ . Although the auxiliary path seems complicated at the first glance, it is equivalent with simulating  $X(t)$  (9) by decomposing each dimension  $d$  into an independent sub-process  $X^d(t)$  whose dynamics are:

$$\frac{d}{dh}\mathbb{P}(X^d(t+h) = e_j | X^d(h) = e_i) = g(\exp(-\langle \nabla_d f(x), e_j - e_i \rangle)) \quad (10)$$

Same as the analysis for a single jump, we know that the first step satisfies  $q(\sigma^1, \sigma^0) \propto g(\exp(-\langle \nabla f(\sigma^0), \sigma^1 - \sigma^0 \rangle))$ . Using the memorylessness of the exponential distribution, when we simulate the  $k$ -th jump conditioned on the  $(k-1)$ -th jump, the property keeps holding for all steps in the auxiliary path. Hence, PAFS is equivalent to simulating the sub-processes  $X^1, \dots, X^D$  until  $L$  jumps occur.

## 4.2 Locally Balanced Jump

One common feature of existing LB samplers is that they restrict the scale of the proposal distributions by the Hamming distance, either flipping one site per M-H step, for LB-1 and GWG, or flipping a fixed number of  $L$  sites per M-H step, for PAFS. Although Zanella (2020), Sun et al. (2021a) have proven its asymptotic optimality for energy based target distributions with Lipschitz energy functions and finite Markov blanket, existing LB samplers ignore the geometric information associated with the energy function in finite dimensional cases. The asymptotic results hold as, in high dimensional spaces, the value of the change rate  $-Q_{xx} = \sum_{y \in N(i)} Q_{xy}$  will weakly converges to a narrow normal random variables, such that simulation with respect to Hamming distance introduces little error. In finite dimensional spaces, however, the concentration no longer holds and the change rate  $-Q_{xx}$  can varies significantly across different states. If  $-Q_{xx} = -2Q_{yy}$  and  $L = 10$  sites has been flipped at state  $y$ , then the gradient flow should flip 20 sites in expectation at state  $x$ . Consequently, a trajectory simulated with a fixed Hamming distance can deviate significantly from the gradient flow. Since the locally balanced dynamics (9) evolve in continuous time, we are inspired to regulate the proposal distribution via the simulation time  $\tau$  rather than Hamming distance. We refer to this new algorithm as the *locally balanced jump* (LBJ).

Identically to PAFS (Sun et al., 2021a), LBJ decomposes the Markov jump process into independent sub-processes  $X^d(t)$ . The difference is that LBJ no longer simulates the indices where the jumps occur. Instead, LBJ directly estimates the transition matrix  $P^d(\tau) \in \mathbb{R}^{n \times n}$  after a simulation time  $\tau$ . In general, a closed form solution of  $P^d(\tau)$  is not available for  $|\mathcal{X}| > 2$ , so LBJ uses an interpolation between  $P^d(0)$  and  $P^d(\infty)$ . Denote  $\theta_{i,j}^d = g(\pi_{x^{d=j}}/\pi_{x^{d=i}})$  and  $\nu_j^d = \pi(x^{d=j})/\sum_{i=1}^n \pi(x^{d=i})$ , where  $x^{d=j} = (x_1, \dots, x_{d-1}, e_j, x_{d+1}, \dots, x_D)$ . Define

$$\left(\tilde{P}^d(\tau)\right)_{i,j} = \begin{cases} \nu_i^d + \sum_{j \neq i} \nu_j^d e^{-\tau \theta_{i,j}^d / \nu_j^d}, & i = j \\ \nu_j^d - \nu_j^d e^{-\tau \theta_{i,j}^d / \nu_j^d} & i \neq j \end{cases} \quad (11)$$

for  $i, j = 1, \dots, n$ . The estimated transition matrix then satisfies  $\tilde{P}^d(0) = P^d(0) = I$ ,  $\tilde{P}^d(\infty) = P^d(\infty) = \nu$ , and  $\frac{d}{dt} \tilde{P}^d(t)|_{t=0} = \frac{d}{dt} P^d(t)|_{t=0}$ . Additionally, when  $|\mathcal{X}| = 2$ , the estimation is exact; that is,  $\tilde{P}^d(\tau) \equiv P^d(\tau)$ . Given the current state  $x$ , LBJ proposes the new state  $y = (y_d)_{d=1}^D$  by sampling each site  $y_d$  according to  $\tilde{P}^d(\tau)$ . In practice, the ratio  $\pi_{x^{d=j}}/\pi_{x^{d=i}}$  can be efficiently approximated by  $\exp(-\langle \nabla f(x), y - x \rangle)$  and each M-H step only requires two evaluations of the energy function and two evaluations of the gradient.

Compared to PAFS, LBJ has advantages in both quality and computation. Regarding quality, LBJ allows location dependent "velocities". That is, if the current state  $x$  has a larger (smaller)  $\theta$ , LBJ will tend to flip more (fewer) sites. In this way, LBJ allows the particle to leave low probability regions more quickly while holding in high probability regions for longer times. Regarding computation, previous LB samplers restrict the scale of the proposal distributions by the Hamming distance. Consequently, they require communication between every dimension. In LBJ, instead, each dimension is simulated independently of the others. Therefore, it allows parallel or even distributed implementations.

Of course, (11) is not the only possible discretization with respect to the simulation time  $\tau$ . Other choices are also possible. For example, one could consider two straightforward approaches: Euler's forward and backward methods. For the forward method, we use the estimate:

$$\tilde{P}_f^d(\tau) = P^d(0) + \tau \frac{d}{dt} P^d(t)|_{t=0} \quad (12)$$

We restrict the simulation time  $\tau$  to make sure that the  $\tilde{P}_f^d(\tau)$  is non-negative, and name this method *LBJf*. For the backward method, we use the estimate :

$$\tilde{P}_b^d(\tau) = P^d(0) + \tau \frac{d}{dt} \tilde{P}^d(t)|_{t=\tau} \quad (13)$$

We employ a numerical method to solve  $\tilde{P}_b^d(\tau)$  and refer to this method as *LBJb*. More details about LBJf and LBJb are given in Appendix B. The forward method LBJf is simple, fast and numerically stable, but typically has poorer approximation quality compared to the backward method LBJb. However, the backward method involves a matrix inverse that can be expensive and numerically unstable when the categorical dimension  $n$  is large. LBJ provides a trade-off between quality and speed. By employing the interpolation, LBJ (11) exhibits proposal quality as good as LBJb with a running speed as fast as LBJf.

## 5 Related Work

Gradient based MCMC algorithms have been extensively studied in continuous spaces (Ma et al., 2015). By simulating Langevin dynamics or Hamiltonian dynamics, the famous MALA (Rosky et al., 1978), HMC (Duane et al., 1987; Neal et al., 2011), and variants (Girolami & Calderhead, 2011; Welling & Teh, 2011; Hoffman et al., 2014) substantially improve the sampling efficiency in both theory and practice. The seminal work of Otto (Jordan et al., 1998; Otto, 2001) shows that the Langevin dynamics simulates the gradient flow on the 2-Wasserstein space  $\mathcal{P}_2(\mathbb{R}^D)$  (Do Carmo & Flaherty Francis, 1992; Villani, 2009). Subsequent work extended the result to Hamiltonian dynamics (Ambrosio & Gangbo, 2008; Liu et al., 2019; Chow et al., 2020), and particle variational inference (Chen et al., 2018; Liu et al., 2019). By contrast, the corresponding theory for discrete spaces is less well understood. Mielke (2011); Maas (2011); Chow et al. (2012) introduce 2-Wasserstein distances on finite graphs via the Benamou-Brenier formula (Benamou & Brenier, 2000) to obtain the Fokker-Planck equation and gradient flow. However, they do not investigate the associated dynamics, and a simulation algorithm at the particle level is unavailable.

A number of samplers for discrete spaces use continuous relaxation. One approach is to map the discrete space to a continuous space, then use a gradient based method to propose a new state in the continuous space, then map the new state back into the original discrete space (Zhang et al., 2012; Pakman & Paninski, 2013; Nishimura et al., 2017; Han et al., 2020; Jaini et al., 2021) via auxiliary variables, uniform dequantization, or VAE flow. Such methods work in some scenarios, but a key challenge is that embedding the discrete space in a continuous space can destroy the inherent discrete structure, resulting in highly multi-modal and irregular target distributions in the continuous space such that defects the performance in high dimensional discrete spaces (Grathwohl et al., 2021).

Another group of methods work directly on discrete spaces. Dai et al. (2020) introduces the path as a latent variable in the variational distribution for initializing PCD, and Titsias & Yau (2017) augment the discrete space with an auxiliary variable. These methods still rely on slow Gibbs sampling for improvement. Recently, a family of locally balanced samplers has shown great success in discrete spaces. Zanella (2020) introduces the point-wise informed proposal  $q(x, y) \propto g(\pi(y)/\pi(x))$  for discrete spaces, and proves that a family of locally balanced functions is asymptotically optimal for  $g$ . Grathwohl et al. (2021) approximate the probability ratio  $\pi(y)/\pi(x)$  by a gradient for scalability. Sun et al. (2021a) introduce an auxiliary path, which allows proposals of distant states, and prove that the locally balanced function is still asymptotically optimal. In this paper, we show that all such locally balanced samplers are simulating the gradient flow in the discrete space. We note that the Markov jump process (8) has been mentioned in previous work (Sohl-Dickstein et al., 2009; Power & Goldman, 2019) but without realizing its connection to the gradient flow.

## 6 Sampling from Classical Energy Based Models

### 6.1 Settings

**Models:** We demonstrate the advantage of LBJ in sampling tasks on four classical models: the Bernoulli model (Bernoulli), Ising model (Ising), factorial hidden Markov model (FHMM), and the restricted Boltzmann machine (RBM). In each model, we use one smooth binary version, one sharp binary version, one smooth categorical version, and one sharp categorical version. Here, smooth and sharp means the model has larger and smaller entropy, respectively. We only present a brief introduction for each model and report the results on smooth versions in this section. More description of the models and additional results are given in Appendix C.

**Baselines:** We consider PAFS (Sun et al., 2021a), the state-of-the-art generic sampler for discrete spaces. We also compare with other samplers: random walk Metropolis (RWM), Hamming Ball sampler (HB) Titsias & Yau (2017), block Gibbs (BG), and Gibbs with Gradient (GWG) Grathwohl

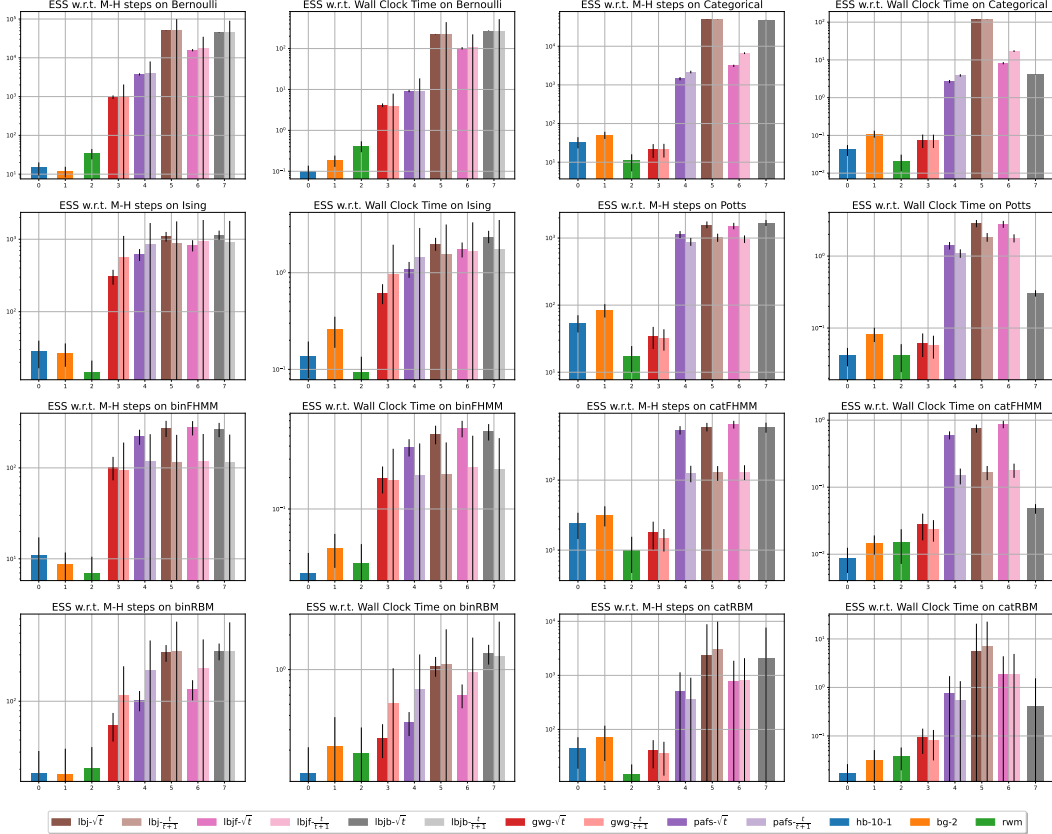


Figure 1: Effective Sample Size on Various Distributions

et al. (2021). Following Grathwohl et al. (2021), we use block size 10 and hamming distance 1 for HB, and use block size 2 for BG. For RWM, GWG, PAFS, and our LBJ, whose proposal distributions are determined by hyperparameters, we tune the scale of the proposal distributions via grid search and report the best results. For locally balanced samplers: GWG, PAFS, and LBJ, we consider two common weight functions  $g(t) = \sqrt{t}$  and  $g(t) = \frac{t}{t+1}$ . We do not report the results for LBJb for  $g(t) = \frac{t}{t+1}$  on categorical models as its matrix inverse is numerically unstable.

**Metrics:** We use effective sample size (ESS) to evaluate each sampler (Lenth, 2001). We report ESS with respect to M-H steps to show the proposal quality and ESS with respect to wall clock time to show the efficiency. For each setting and each method, we run 100 chains for 100,000 steps. We calculate the ESS using the last 50,000 steps and report mean and standard deviation.

## 6.2 Results

**Bernoulli and Categorical:** The Bernoulli distribution is the simplest distribution in a discrete space, consisting of independent binary random variables. The categorical distribution is a simple generalization to categorical random variables. For  $x \in \mathcal{X}^D$ , the energy function is:

$$f(x) = \sum_{d=1}^D \langle x_d, \theta_d \rangle \quad (14)$$

We report the results in the first row of Figure 1. We can see that the LBJ samplers perform systematically better than the LB samplers. LBJ and LBJb demonstrate significantly better proposal quality than the other samplers. However, LBJb is less efficient on the categorical model, as the matrix inverse is time consuming. We also note that the weight function  $g(t) = \frac{t}{t+1}$  performs consistently better than  $g(t) = \sqrt{t}$ , as proven in Zanella (2020).

**Ising and Potts:** The Ising model (Cipra, 1987) is a mathematical model of ferromagnetism in statistical mechanics. It consists of binary random variables arranged in a lattice graph  $G = ([D], E)$  and allows each node to interact with its neighbors. The Potts model (Wu, 1982) is a generalization of the Ising model where the random variables are categorical. The energy function is:

$$f(x) = - \sum_{d=1}^D \langle x_d, \theta_d \rangle - \lambda \sum_{(i,j) \in E} \delta(x_i, x_j) \quad (15)$$

We report the results in the second row of Figure 1. We can see that all LB samplers exhibit good performance. Among them, LBJ and LBJf are the most efficient. The weight functions  $g(t) = \sqrt{t}$  and  $g(t) = \frac{t}{1+t}$  each demonstrate advantages for different samplers.

**FHMM:** FHMM (Ghahramani & Jordan, 1995) uses latent variables to characterize time series data. In particular, it assumes the continuous data  $y \in \mathbb{R}^L$  is generated by hidden state  $x \in \mathcal{X}^{L \times K \times n}$ , where we use  $n = 2$  for the binary FHMM (binFHMM) and  $n = 4, 8$  for the categorical FHMM (catFHMM). The probability function is:

$$p(x) = p(x_1) \prod_{l=2}^L p(x_l | x_{l-1}), \quad p(y|x) = \prod_{l=1}^L \mathcal{N}(y_l; \sum_{k=1}^K \langle W_k, x_{l,k} \rangle + b; \sigma^2) \quad (16)$$

We report the results in the third row of Figure 1. Similar to the Ising model, we can see that all locally balanced samplers demonstrate good performance. In FHMM, PAFS has an efficiency very close to the LBJ samplers. We believe this is because the energy change rate is stable in FHMM and the magnitude of the gradient changes steadily. Hence the Hamming distance works as a good metric. We also note that the weight function  $g(t) = \sqrt{t}$  is systematically better than  $g(t) = \frac{t}{t+1}$  on FHMM. This is consistent with the observation in Livingstone & Zanella (2019) that  $g(t) = \sqrt{t}$  performs better on smooth target distributions and  $g(t) = \frac{t}{t+1}$  performs better on nonsmooth target distributions, although Livingstone & Zanella (2019) focus on the sampling in continuous spaces.

**RBM:** The RBM is an unnormalized latent variable model, with a visible random variable  $v \in \mathcal{X}^D$  and a hidden random variable  $h \in \{0, 1\}^M$ . When  $v$  is binary, we call it a binary RBM (binRBM) and when  $v$  is categorical, we call it a categorical RBM (catRBM). The energy function is:

$$f(v, h) = - \sum_{d=1}^D \langle v_d, \theta_d \rangle - \sum_{m=1}^M \beta_m h_m - \sum_{d,m} \langle h_m \theta_{m,d}, v_d \rangle \quad (17)$$

Unlike the previous three models, where the parameters are hand designed, we train binary RBM on MNIST (LeCun et al., 1998) and categorical RBM on Fashion-MNIST (Xiao et al., 2017) using contrastive divergence Hinton (2002). We show the results for the smooth model in the third row of Figure 1. The learned RBMs have stronger multi-modality compared to previous models. We can see that, as before, LBJ and LBJb lead in proposal quality, while LBJ is the most efficient overall.

## 7 Learning Deep Energy Based Models

Deep energy-based models (EBMs) have gained increasing popularity for generative modeling. Recent advances including tempered Langevin samplers (Nijkamp et al., 2020), large persistent chains (Du & Mordatch, 2019), and amortized sampling (Dai et al., 2019, 2020), which have enabled deep EBMs to become a competitive approach for image generation (Song et al., 2020), retrosynthesis (Sun et al., 2021b), molecule design (Xie et al., 2021), language modelling (Bakhtin et al., 2021) and many other problems. Learning an EBM is challenging. Given data sampled from a true distribution  $\pi$ , we maximize the likelihood of the target distribution  $\pi_\theta(x) \propto e^{-f_\theta(x)}$  parameterized by  $\theta$ . The gradient of the likelihood is:

$$\nabla_\theta \log \pi_\theta(x) = \mathbb{E}_\pi[\nabla_\theta f_\theta(x)] - \mathbb{E}_{\pi_\theta}[\nabla_\theta f_\theta(x)] \quad (18)$$

The first expectation can be estimated using the data from the true distribution. The second expectation requires samples from the current model, which are typically obtained via MCMC. The speed of EBM training is determined by how fast the MCMC algorithm can obtain a good estimate of the second expectation. Following Grathwohl et al. (2021) and Sun et al. (2021a), we train deep EBMs parameterized by residual networks (He et al., 2016) on binary and grayscale image datasets using PCD (Tieleman, 2008) with a replay buffer (Du & Mordatch, 2019). The grayscale images were treated as 1-of-256 categorical data.

Data Type	Dataset	VAE (MLP)	VAE (Conv)	RBM	DBN	EBM (GWG)	EBM (Gibbs)	EBM (PAS)	EBM (LBJf)	EBM (LBJ)
Binary log-likelihood $\uparrow$	Static MNIST	-86.05	-82.41	-86.39	-85.67	-80.01	-117.17	-79.58	<b>-79.11</b>	-79.13
	Dynamic MNIST	-82.42	-80.40	—	—	-80.51	-121.19	-79.59	-79.90	<b>-78.84</b>
	Omniglot	-103.52	97.65	-100.47	-100.78	-94.72	-142.06	<b>-90.75</b>	-91.03	-90.84
Categorical (bits/dim $\downarrow$ )	Caltech Silhouettes	-112.08	-106.35	—	—	-96.20	163.50	-84.56	<b>-75.19</b>	-77.04
	Frey Faces	4.61	4.49	—	—	4.65	—	4.74	<b>4.26</b>	4.33
	Histopathology	5.82	5.59	—	—	5.08	—	5.1	<b>4.84</b>	4.91

Table 1: Evaluation of effectiveness on learning both binary and categorical EBMs.

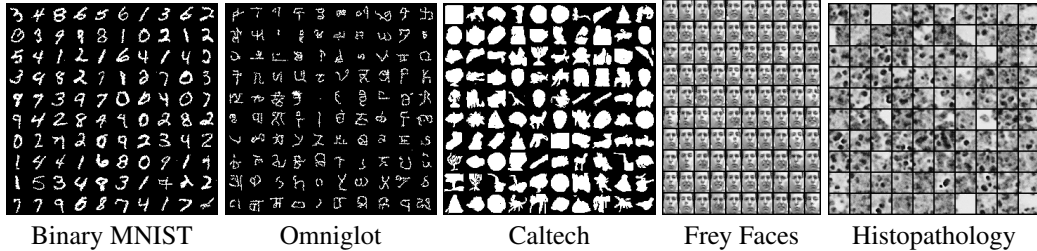


Figure 2: Samples from learned deep EBMs using proposed LBJ sampler.

We present the test-set likelihoods in Table 1. Likelihoods are estimated using annealed importance sampling (Neal, 2001). We compare the performance of the LBJ and LBJf samplers, with weight function  $g(t) = \sqrt{t}$ , to Variational Autoencoder (Kingma & Welling, 2013), an RBMM, a deep belief network (DBN) (Hinton, 2009) and EBMs trained by Gibbs, GWG (Grathwohl et al., 2021), and PAFS (Sun et al., 2021a). We do not include LBJb as it requires inversion of  $256 \times 256$  matrices and is computationally prohibitive. On most of datasets, the LBJ and LBJf samplers enable deep EBMs to become competitive on high dimensional discrete data. One observation is that LBJf obtains slightly better likelihood than LBJ. We believe the reason is that LBJf is numerically more stable in dealing with complicated deep EBMs. We also present long-run samples from the trained models in Figure 2.

## 8 Discussion

In this paper, we proposed the locally balanced dynamics and showed that it simulates Wasserstein gradient flows in a discrete distribution space. Such a framework explains the good performance of previous locally balanced samplers. More importantly, in this generic framework, we propose a new algorithm *locally balanced jump* (LBJ) that further improves the efficiency in both sampling and learning tasks across various distributions. Despite the success of LBJ in this paper, there are still a lot of interesting problems to investigate.

**Weight function:** every locally balanced function  $g(t)$  determines a locally balanced dynamic. In this paper, we only empirically evaluated the most commonly used  $g(t) = \sqrt{t}$  and  $g(t) = \frac{t}{t+1}$  and found that each has its own advantages on different models. Livingstone & Zanella (2019) shows  $g(t) = \frac{t}{t+1}$  is more robust than  $g(t) = \sqrt{t}$  on non-smooth distributions in continuous spaces. Sansone (2021) attempts to learn the locally balanced function in a discrete space. We believe that locally balanced dynamics provides a new angle to analyze this problem via the gradient flow.

**Discretization:** previous locally balanced samplers simulate the time when the jumps happen. In this work, we employ the Euler forward (12), Euler backward (13), and a hand design interpolation (11) to estimate the transition matrix after simulation time  $\tau$ . There exist many different approaches that might provide a better trade-off between approximation quality and computational cost. For example, considering fruitful numerical methods like Heun’s method and Runge–Kutta method, we believe there is ample room to improve discretization.

**Dynamics:** Locally balanced dynamics can be seen as a discrete version of Langevin dynamics. There also exist other dynamics in continuous space, for example, Hamiltonian dynamics. An interesting question is whether a discrete version of Hamiltonian dynamics exists. Second, as mentioned in Section 3.2, the Wasserstein gradient flow is a special case of the Fokker-Planck equation in discrete spaces, where the free energy is defined as the KL-divergence:  $F(\rho) = \sum_i \rho_i f_i + \sum_i \rho_i \log \rho_i$ . The

free energy  $F(\rho)$  can be chosen in other forms, such as quadratic:  $F(\rho) = \sum_i \rho_i f_i + \sum_{i,j} \rho_i \rho_j W_{ij}$ . How to efficiently simulate the general Fokker-Planck equation in discrete spaces is still unknown.

Overall, the locally balanced dynamics provide a new framework for studying generic sampling algorithms in discrete spaces. We believe this is a milestone for sampling in discrete spaces and expect further development of sampling algorithms in this framework.

## References

- Ambrosio, L. and Gangbo, W. Hamiltonian odes in the wasserstein space of probability measures. *Communications on Pure and Applied Mathematics: A Journal Issued by the Courant Institute of Mathematical Sciences*, 61(1):18–53, 2008.
- Bakhtin, A., Deng, Y., Gross, S., Ott, M., Ranzato, M., and Szlam, A. Residual energy-based models for text. *J. Mach. Learn. Res.*, 22:40–1, 2021.
- Benamou, J.-D. and Brenier, Y. A computational fluid mechanics solution to the monge-kantorovich mass transfer problem. *Numerische Mathematik*, 84(3):375–393, 2000.
- Chen, C., Zhang, R., Wang, W., Li, B., and Chen, L. A unified particle-optimization framework for scalable bayesian sampling. *arXiv preprint arXiv:1805.11659*, 2018.
- Cheng, X. and Bartlett, P. Convergence of langevin mcmc in kl-divergence. In *Algorithmic Learning Theory*, pp. 186–211. PMLR, 2018.
- Chow, S.-N., Huang, W., Li, Y., and Zhou, H. Fokker–planck equations for a free energy functional or markov process on a graph. *Archive for Rational Mechanics and Analysis*, 203(3):969–1008, 2012.
- Chow, S.-N., Li, W., and Zhou, H. Entropy dissipation of fokker-planck equations on graphs. *arXiv preprint arXiv:1701.04841*, 2017.
- Chow, S.-N., Li, W., and Zhou, H. Wasserstein hamiltonian flows. *Journal of Differential Equations*, 268(3):1205–1219, 2020.
- Cipra, B. A. An introduction to the ising model. *The American Mathematical Monthly*, 94(10): 937–959, 1987.
- Dai, B., Liu, Z., Dai, H., He, N., Gretton, A., Song, L., and Schuurmans, D. Exponential family estimation via adversarial dynamics embedding. *Advances in Neural Information Processing Systems*, 32, 2019.
- Dai, H., Singh, R., Dai, B., Sutton, C., and Schuurmans, D. Learning discrete energy-based models via auxiliary-variable local exploration. *Advances in Neural Information Processing Systems*, 33: 10443–10455, 2020.
- Do Carmo, M. P. and Flaherty Francis, J. *Riemannian geometry*, volume 6. Springer, 1992.
- Du, Y. and Mordatch, I. Implicit generation and generalization in energy-based models. *arXiv preprint arXiv:1903.08689*, 2019.
- Duane, S., Kennedy, A. D., Pendleton, B. J., and Roweth, D. Hybrid monte carlo. *Physics letters B*, 195(2):216–222, 1987.
- Ghahramani, Z. and Jordan, M. Factorial hidden markov models. *Advances in Neural Information Processing Systems*, 8, 1995.
- Gillespie, D. T. Exact stochastic simulation of coupled chemical reactions. *The journal of physical chemistry*, 81(25):2340–2361, 1977.
- Girolami, M. and Calderhead, B. Riemann manifold langevin and hamiltonian monte carlo methods. *Journal of the Royal Statistical Society: Series B (Statistical Methodology)*, 73(2):123–214, 2011.
- Grathwohl, W., Swersky, K., Hashemi, M., Duvenaud, D., and Maddison, C. J. Oops i took a gradient: Scalable sampling for discrete distributions. *arXiv preprint arXiv:2102.04509*, 2021.

- Han, J., Ding, F., Liu, X., Torresani, L., Peng, J., and Liu, Q. Stein variational inference for discrete distributions. In *International Conference on Artificial Intelligence and Statistics*, pp. 4563–4572. PMLR, 2020.
- He, K., Zhang, X., Ren, S., and Sun, J. Deep residual learning for image recognition. In *Proceedings of the IEEE conference on computer vision and pattern recognition*, pp. 770–778, 2016.
- Hinton, G. E. Training products of experts by minimizing contrastive divergence. *Neural computation*, 14(8):1771–1800, 2002.
- Hinton, G. E. Deep belief networks. *Scholarpedia*, 4(5):5947, 2009.
- Hoffman, M. D., Gelman, A., et al. The no-u-turn sampler: adaptively setting path lengths in hamiltonian monte carlo. *J. Mach. Learn. Res.*, 15(1):1593–1623, 2014.
- Jaini, P., Nielsen, D., and Welling, M. Sampling in combinatorial spaces with survae flow augmented mcmc. In *International Conference on Artificial Intelligence and Statistics*, pp. 3349–3357. PMLR, 2021.
- Johnson, C. R. and Smith, R. L. Inverse m-matrices, ii. *Linear algebra and its applications*, 435(5): 953–983, 2011.
- Jordan, R., Kinderlehrer, D., and Otto, F. The variational formulation of the fokker–planck equation. *SIAM journal on mathematical analysis*, 29(1):1–17, 1998.
- Kingma, D. P. and Welling, M. Auto-encoding variational bayes. *arXiv preprint arXiv:1312.6114*, 2013.
- LeCun, Y., Bottou, L., Bengio, Y., and Haffner, P. Gradient-based learning applied to document recognition. *Proceedings of the IEEE*, 86(11):2278–2324, 1998.
- Lenth, R. V. Some practical guidelines for effective sample size determination. *The American Statistician*, 55(3):187–193, 2001.
- Liu, C., Zhuo, J., and Zhu, J. Understanding mcmc dynamics as flows on the wasserstein space. In *International Conference on Machine Learning*, pp. 4093–4103. PMLR, 2019.
- Livingstone, S. and Zanella, G. The barker proposal: combining robustness and efficiency in gradient-based mcmc. *arXiv preprint arXiv:1908.11812*, 2019.
- Ma, Y.-A., Chen, T., and Fox, E. A complete recipe for stochastic gradient mcmc. *Advances in neural information processing systems*, 28, 2015.
- Maas, J. Gradient flows of the entropy for finite markov chains. *Journal of Functional Analysis*, 261(8):2250–2292, 2011.
- Mielke, A. A gradient structure for reaction–diffusion systems and for energy-drift-diffusion systems. *Nonlinearity*, 24(4):1329, 2011.
- Neal, R. M. Annealed importance sampling. *Statistics and computing*, 11(2):125–139, 2001.
- Neal, R. M. et al. Mcmc using hamiltonian dynamics. *Handbook of markov chain monte carlo*, 2(11):2, 2011.
- Nijkamp, E., Hill, M., Han, T., Zhu, S.-C., and Wu, Y. N. On the anatomy of mcmc-based maximum likelihood learning of energy-based models. In *Proceedings of the AAAI Conference on Artificial Intelligence*, volume 34, pp. 5272–5280, 2020.
- Nishimura, A., Dunson, D., and Lu, J. Discontinuous hamiltonian monte carlo for sampling discrete parameters. *arXiv preprint arXiv:1705.08510*, 853, 2017.
- Otto, F. The geometry of dissipative evolution equations: the porous medium equation. 2001.
- Pakman, A. and Paninski, L. Auxiliary-variable exact hamiltonian monte carlo samplers for binary distributions. *arXiv preprint arXiv:1311.2166*, 2013.

- Power, S. and Goldman, J. V. Accelerated sampling on discrete spaces with non-reversible markov processes. *arXiv preprint arXiv:1912.04681*, 2019.
- Robert, C. and Casella, G. *Monte Carlo statistical methods*. Springer Science & Business Media, 2013.
- Rossky, P. J., Doll, J., and Friedman, H. Brownian dynamics as smart monte carlo simulation. *The Journal of Chemical Physics*, 69(10):4628–4633, 1978.
- Sansone, E. Lsb: Local self-balancing mcmc in discrete spaces. *arXiv preprint arXiv:2109.03867*, 2021.
- Sohl-Dickstein, J., Battaglino, P., and DeWeese, M. R. Minimum probability flow learning. *arXiv preprint arXiv:0906.4779*, 2009.
- Song, Y., Sohl-Dickstein, J., Kingma, D. P., Kumar, A., Ermon, S., and Poole, B. Score-based generative modeling through stochastic differential equations. *arXiv preprint arXiv:2011.13456*, 2020.
- Sun, H., Dai, H., Xia, W., and Ramamurthy, A. Path auxiliary proposal for mcmc in discrete space. In *International Conference on Learning Representations*, 2021a.
- Sun, R., Dai, H., Li, L., Kearnes, S., and Dai, B. Towards understanding retrosynthesis by energy-based models. *Advances in Neural Information Processing Systems*, 34, 2021b.
- Tieleman, T. Training restricted boltzmann machines using approximations to the likelihood gradient. In *Proceedings of the 25th international conference on Machine learning*, pp. 1064–1071, 2008.
- Titsias, M. K. and Yau, C. The hamming ball sampler. *Journal of the American Statistical Association*, 112(520):1598–1611, 2017.
- Tran, T., Phung, D., and Venkatesh, S. Mixed-variate restricted boltzmann machines. In *Asian conference on machine learning*, pp. 213–229. PMLR, 2011.
- Villani, C. *Optimal transport: old and new*, volume 338. Springer, 2009.
- Welling, M. and Teh, Y. W. Bayesian learning via stochastic gradient langevin dynamics. In *Proceedings of the 28th international conference on machine learning (ICML-11)*, pp. 681–688. Citeseer, 2011.
- Wu, F.-Y. The potts model. *Reviews of modern physics*, 54(1):235, 1982.
- Xiao, H., Rasul, K., and Vollgraf, R. Fashion-mnist: a novel image dataset for benchmarking machine learning algorithms, 2017.
- Xie, Y., Shi, C., Zhou, H., Yang, Y., Zhang, W., Yu, Y., and Li, L. Mars: Markov molecular sampling for multi-objective drug discovery. *arXiv preprint arXiv:2103.10432*, 2021.
- Zanella, G. Informed proposals for local mcmc in discrete spaces. *Journal of the American Statistical Association*, 115(530):852–865, 2020.
- Zhang, Y., Ghahramani, Z., Storkey, A. J., and Sutton, C. Continuous relaxations for discrete hamiltonian monte carlo. *Advances in Neural Information Processing Systems*, 25:3194–3202, 2012.

## A Complete Proofs

### A.1 Lemma 3.1

Consider  $V = \{1, \dots, M\}$ . Denote  $F(G)$  as the set of all vector fields on graph  $G$ . The divergence operator  $\text{div}_\rho$  maps a vector field  $v \in F(G)$  to a vector  $\sigma$  in the tangent space  $T_\rho\mathcal{P}(V)$ . It is not hard to see that  $\text{div}_\rho$  is a surjection, but not an injection. For a  $\sigma \in T_\rho\mathcal{P}(V)$ , there are infinite choices of vector field  $v$  such that  $\text{div}_\rho(v) = \sigma$ . Lemma 3.1 tells us that for Wasserstein distance defined in (3), we only need to consider vector field  $v$  as a potential field.

*Proof.* We show that given arbitrary vector field  $u$ , there exists a potential field  $\nabla\Phi$  has the same divergence and minimizes the norm. In particular, let us consider the following optimization problem:

$$\min_v \langle v, v \rangle, \quad \text{subject to: } \text{div}_\rho(v) = \text{div}_\rho(u) = \sigma \quad (19)$$

We introduce the dual variable  $(\lambda_i)_{i=1}^M$  and we have the Lagrangian:

$$L(v, \Phi) = \sum_{(i,j) \in E} g_{ij} v_{ij}^2 + \sum_{i=1}^M \Phi_i (\sigma_i - \sum_{j \in N(i)} g_{ji} v_{ji} - g_{ij} v_{ij}) \quad (20)$$

$$= \sum_{(i,j) \in E} [(\lambda_i - \lambda_j) + v_{ij}] g_{ij} v_{ij} + \sum_{i=1}^M \lambda_i \sigma_i \quad (21)$$

Since  $u$  is a solution, the optimization problem (19) is feasible. Since the inner product  $\langle v, v \rangle \geq 0$ , the optimization problem (19) is bounded. By Slater's condition, the strong duality holds and the Lagrangian is minimized at  $(v^*, \lambda^*)$  with a finite value. Hence, we have  $v_{ij}^* = \lambda_j^* - \lambda_i^*$ . When we let  $\Phi_i = \lambda_i^*$ , we have  $v^* = \nabla\Phi$  is a potential field.  $\square$

### A.2 Lemma 3.2

Lemma 3.1 tells us that the minimum vector field to realize a divergence is in the form of a potential field. We can notice that a potential field is invariant up to a constant shifting. That's to say, if  $\Phi$  is a potential function and  $\Phi' = \Phi + c = (\Phi_i + c)_{i=1}^M$ , then  $\nabla\Phi' = \nabla\Phi$ . Hence, we consider an equivalence class  $[\Phi] = \{\Phi' \in \mathbb{R}^M : \exists c \in \mathbb{R}, \Phi' = \Phi + c\}$  and we denote  $P^M = \{[\Phi] : \Phi \in \mathbb{R}^M\}$ . Then, lemma 3.2 gives an isomorphism between  $P^M$  and  $T_\rho\mathcal{P}(V)$ .

*Proof.* We first show  $\zeta([\Phi]) = \text{div}_\rho(\nabla\Phi)$  is well-defined. For arbitrary  $\Phi^1, \Phi^2 \in [\Phi]$ , we have  $\nabla\Phi^1 = \nabla\Phi^2$ , thereby  $\text{div}_\rho(\nabla\Phi^1) = \text{div}_\rho(\nabla\Phi^2)$ . It indicates  $\zeta$  is well-defined.

Second, we show  $\zeta$  is linear. We have

$$\zeta(\alpha[\Phi^1] + \beta[\Phi^2]) = \zeta([\alpha\Phi^1 + \beta\Phi^2]) \quad (22)$$

$$= \text{div}_\rho(\nabla(\alpha\Phi^1 + \beta\Phi^2)) \quad (23)$$

$$= \alpha \text{div}_\rho(\nabla\Phi^1) + \beta \text{div}_\rho(\nabla\Phi^2) \quad (24)$$

$$= \alpha\zeta([\Phi^1]) + \beta\zeta([\Phi^2]) \quad (25)$$

We have (22) holds as

$$\psi \in \alpha[\Phi^1] + \beta[\Phi^2] \iff \exists c^1, c^2, \psi = \alpha(\Phi^1 + c^1) + \beta(\Phi^2 + c^2) \quad (26)$$

$$\iff \exists c, \psi = \alpha\Phi^1 + \beta\Phi^2 + c \quad (27)$$

$$\iff \psi \in [\alpha\Phi^1 + \beta\Phi^2] \quad (28)$$

Third, we show that  $\zeta$  is an injection. By the property shown above, we have

$$\zeta([\Phi^1]) = \zeta([\Phi^2]) \iff \zeta([\Phi^1 - \Phi^2]) = 0 \quad (29)$$

That means for any  $(i, j) \in E$

$$(\Phi^1 - \Phi^2)_j - (\Phi^1 - \Phi^2)_i = 0 \quad (30)$$

Since we assume  $G$  is connected, it indicates  $\Phi^1 = \Phi^2 + c$ , hence  $[\Phi^1] = [\Phi^2]$ . As both  $P^M$  and  $T_\rho\mathcal{P}(V)$  are linear space with dimension  $M - 1$ , we prove  $\zeta$  is a linear isomorphism.  $\square$

### A.3 Definition 3.3

Lemma 3.2 gives an immersion (Do Carmo & Flaherty Francis, 1992) from the tangent space  $T_\rho \mathcal{P}(V)$  to the set of vector fields  $F(G)$ . Since we define the inner-product on  $F(G)$  in (2),  $\zeta$  naturally induce the metric on  $T_\rho \mathcal{P}(V)$ . In this section, we will first justify  $\langle \sigma^1, \sigma^2 \rangle_\rho$  is valid. Assume  $\Phi^{\sigma^2}, \Psi^{\sigma^2} \in \zeta^{-1}(\sigma^2)$ , then there exists  $c$ , such that  $\Phi^{\sigma^2} = \Psi^{\sigma^2} + c$ . Hence we have:

$$\sum_{i=1}^M \sigma_i^1 (\Phi_i^{\sigma^2} - \Psi_i^{\sigma^2}) = c \sum_{i=1}^M \sigma_i^1 = 0 \quad (31)$$

It shows that the value of  $\langle \sigma^1, \sigma^2 \rangle_\rho$  does not depend on the choice of the representative  $\Phi^{\sigma^2}$ , hence it is well-defined.

To show  $\langle \sigma^1, \sigma^2 \rangle_\rho$  is a valid inner-product, we need to check conjugate symmetry, linearity in the first argument, and positive-definiteness. For conjugate symmetry, we have:

$$\langle \sigma^2, \sigma^1 \rangle_\rho = \sum_{i=1}^M \sigma_i^2 \Phi_i^{\sigma^1} \quad (32)$$

$$= \sum_{i=1}^M \operatorname{div}_\rho(\nabla \Phi^{\sigma^1})_i \Phi_i^{\sigma^1} \quad (33)$$

$$= \sum_{i=1}^M \sum_{j \in N(i)} g_{ij}(\rho) (\Phi_i^{\sigma^1} - \Phi_j^{\sigma^1}) \Phi_i^{\sigma^2} \quad (34)$$

$$= \frac{1}{2} \sum_{i=1}^M \sum_{j \in N(i)} g_{ij}(\rho) (\Phi_i^{\sigma^1} - \Phi_j^{\sigma^1}) \Phi_i^{\sigma^2} + \frac{1}{2} \sum_{j=1}^M \sum_{i \in N(j)} g_{ij}(\rho) (\Phi_i^{\sigma^1} - \Phi_j^{\sigma^1}) \Phi_i^{\sigma^2} \quad (35)$$

$$= \frac{1}{2} \sum_{i=1}^M \Phi_i^{\sigma^2} \sum_{j \in N(i)} g_{ij}(\rho) (\Phi_i^{\sigma^1} - \Phi_j^{\sigma^1}) + \frac{1}{2} \sum_{j=1}^M \Phi_j^{\sigma^2} \sum_{i \in N(j)} g_{ij}(\rho) (\Phi_i^{\sigma^1} - \Phi_j^{\sigma^1}) \quad (36)$$

$$= \frac{1}{2} \sum_{i=1}^M \Phi_i^{\sigma^2} \sum_{j \in N(i)} g_{ij}(\rho) (\Phi_i^{\sigma^1} - \Phi_j^{\sigma^1}) + \frac{1}{2} \sum_{i=1}^M \Phi_i^{\sigma^2} \sum_{j \in N(i)} g_{ij}(\rho) (\Phi_j^{\sigma^1} - \Phi_i^{\sigma^1}) \quad (37)$$

$$= \frac{1}{2} \sum_{(i,j) \in E} g_{ij}(\rho) (\Phi_i^{\sigma^1} - \Phi_j^{\sigma^1}) (\Phi_i^{\sigma^2} - \Phi_j^{\sigma^2}) \quad (38)$$

We can see that (38) does not depend on the order of  $\sigma^1$  and  $\sigma^2$ , hence we have:

$$\langle \sigma^1, \sigma^2 \rangle = \langle \sigma^2, \sigma^1 \rangle \quad (39)$$

The linearity for the first argument is trivial to see. For positive-definiteness, if we have  $\langle \sigma, \sigma \rangle_\rho = 0$ , then by (38), we have:

$$\sum_{(i,j) \in E} g_{ij}(\rho) (\Phi_i^\sigma - \Phi_j^\sigma)^2 = 0 \quad (40)$$

Since by our assumption,  $G$  is connected and  $g_{ij}(\rho) > 0$ , it indicates  $\sigma = \nabla \Phi^\sigma = 0$ . Finally, from (38), we can see that:

$$\langle \sigma^1, \sigma^2 \rangle_\rho = \langle \nabla \Phi^{\sigma^1}, \nabla \Phi^{\sigma^2} \rangle_\rho \quad (41)$$

This means the inner-product we defined in (4) is compatible with the immersion  $\zeta$ .

### A.4 Theorem 3.5

We prove the theorem in a more general form in terms of free energy  $F : \mathcal{P}_2(V) \rightarrow \mathbb{R}$ . Once we find the gradient flow for  $F$ , theorem 3.5 can be seen as a special case. In particular, when we define

$$F(\rho) = \sum_{i=1}^M \rho_i f_i - \sum_{i=1}^M \rho_i \log \rho_i \quad (42)$$

we have  $F(\rho) = D_{\text{KL}}(\rho || \pi)$ .

*Proof.* The gradient flow in terms of the free energy is:

$$\frac{d\rho}{dt} = -\nabla_{\rho}F(\rho) \quad (43)$$

By lemma 3.2, for any  $\sigma \in T_{\rho}\mathcal{P}_2(V)$ , we have  $\Phi^{\sigma} \in \zeta^{-1}(\sigma)$  such that  $\sigma = \text{div}_{\rho}(\Phi^{\sigma})$ . On the left hand side, we have:

$$\left\langle \frac{d\rho}{dt}, \sigma \right\rangle = \sum_{i=1}^M \frac{d\rho_i}{dt} \Phi_i^{\sigma} \quad (44)$$

On the right hand side, we have:

$$\langle \nabla_{\rho}F(\rho), \sigma \rangle = \sum_{i=1}^M \frac{\partial F(\rho)}{\partial \rho_i} \sum_{j \in N(i)} g_{ij}(\rho) (\Phi_i^{\sigma} - \Phi_j^{\sigma}) \quad (45)$$

$$= \sum_{i=1}^M \frac{\partial F(\rho)}{\partial \rho_i} \sum_{j \in N(i)} g_{ij}(\rho) \Phi_i^{\sigma} - \sum_{i=1}^M \frac{\partial F(\rho)}{\partial \rho_i} \sum_{j \in N(i)} g_{ij}(\rho) \Phi_j^{\sigma} \quad (46)$$

$$= \sum_{i=1}^M \Phi_i^{\sigma} \sum_{j \in N(i)} g_{ij}(\rho) \frac{\partial F(\rho)}{\partial \rho_i} - \sum_{j=1}^M \Phi_j^{\sigma} \sum_{i \in N(j)} g_{ij}(\rho) \frac{\partial F(\rho)}{\partial \rho_i} \quad (47)$$

$$= \sum_{i=1}^M \Phi_i^{\sigma} \sum_{j \in N(i)} g_{ij}(\rho) \frac{\partial F(\rho)}{\partial \rho_i} - \sum_{i=1}^M \Phi_i^{\sigma} \sum_{j \in N(i)} g_{ij}(\rho) \frac{\partial F(\rho)}{\partial \rho_j} \quad (48)$$

$$= \sum_{i=1}^m \left( \sum_{j \in N(i)} g_{ij}(\rho) \left( \frac{\partial F(\rho)}{\partial \rho_i} - \frac{\partial F(\rho)}{\partial \rho_j} \right) \right) \Phi_i^{\sigma} \quad (49)$$

Hence we have:

$$\sum_{i=1}^M \frac{d\rho_i}{dt} \Phi_i^{\sigma} = - \sum_{i=1}^m \left( \sum_{j \in N(i)} g_{ij}(\rho) \left( \frac{\partial F(\rho)}{\partial \rho_i} - \frac{\partial F(\rho)}{\partial \rho_j} \right) \right) \Phi_i^{\sigma} \quad (50)$$

holds for arbitrary  $\Phi^{\sigma}$ . Then we prove:

$$\frac{d\rho_i}{dt} = \sum_{j \in N(i)} g_{ij}(\rho) \left( \frac{\partial F(\rho)}{\partial \rho_j} - \frac{\partial F(\rho)}{\partial \rho_i} \right) \quad (51)$$

Plug in the value of free energy in (42), we have:

$$\frac{d\rho_i}{dt} = \sum_{j \in N(i)} g_{ij}(\rho) f_j + \log \rho_j - f_i - \log \rho_i \quad (52)$$

Thus we prove the theorem.  $\square$

## B Sampler Details

In this section, we discuss different discretizations for LBJ. In particular, we decomposes the Markov jump process into independent sub-processes  $X^d(t)$ , whose distribution satisfies to the ODE:

$$\frac{d}{dt}\rho^d(t) = \rho^d(t)Q^d \quad (53)$$

where the generator satisfies:

$$Q^d = \begin{bmatrix} -\sum_{j \neq 1} \theta_{1,j}^d & \theta_{1,2}^d & \cdots & \theta_{1,n-1}^d & \theta_{1,n}^d \\ \theta_{2,1}^d & -\sum_{j \neq 2} \theta_{2,j}^d & \cdots & \theta_{2,n-1}^d & \theta_{2,n}^d \\ \vdots & \vdots & \ddots & \vdots & \vdots \\ \theta_{n,1}^d & \theta_{n,2}^d & \cdots & \theta_{n,n-1}^d & -\sum_{j \neq n} \theta_{n,j}^d \end{bmatrix} \quad (54)$$

In following, we will show how LBJ, LBJf, LBJb use interpolation, forward Euler, backward Euler, respectively, to estimation the distribution  $\rho^d$ .

### B.1 Different Discretizations

**LBJ as Interpolation.** Our LBJ estimate the transition matrix via an interpolation between the initial Dirac distribution towards the stationary distribution in each dimension  $d$ . We describe the transition matrix in (11). The matrix form can be written as:

$$\tilde{P}(\tau) = \begin{bmatrix} \nu_1 + \sum_{j \neq 1} \nu_j e^{-\tau \frac{\theta_{1,j}}{\nu_j}} & \nu_2 - \nu_2 e^{-\tau \frac{\theta_{1,2}}{\nu_2}} & \cdots & \nu_n - \nu_n e^{-\tau \frac{\theta_{1,n}}{\nu_n}} \\ \nu_1 - \nu_1 e^{-\tau \frac{\theta_{2,1}}{\nu_1}} & \nu_2 + \sum_{j \neq 2} \nu_j e^{-\tau \frac{\theta_{2,j}}{\nu_j}} & \cdots & \nu_n - \nu_n e^{-\tau \frac{\theta_{2,n}}{\nu_n}} \\ \vdots & \vdots & \ddots & \vdots \\ \nu_1 - \nu_1 e^{-\tau \frac{\theta_{n,1}}{\nu_1}} & \nu_2 - \nu_2 e^{-\tau \frac{\theta_{n,2}}{\nu_2}} & \cdots & \nu_n + \sum_{j \neq n} \nu_j e^{-\tau \frac{\theta_{n,j}}{\nu_j}} \end{bmatrix} \quad (55)$$

We can easily verify that  $\tilde{P}(0) = I = P(0)$ , and each row  $\tilde{P}_i(\infty) = \nu = P_i(\infty)$  converges to the stationary distribution of (53). Moreover,  $\tilde{P}(\tau)$  has the same first order approximation as  $P(\tau)$  at  $\tau = 0$ , since

$$\frac{d}{dt}\tilde{P}^d(t)|_{t=0} = Q^d = \frac{d}{dt}P^d(t)|_{t=0} \quad (56)$$

A special case is  $n = 2$ . When the model is binary, we have:

$$\tilde{P}(\tau) = \begin{bmatrix} \nu_1 + \nu_2 e^{-\tau \frac{\theta_{1,2}}{\nu_2}} & \nu_2 - \nu_2 e^{-\tau \frac{\theta_{1,2}}{\nu_2}} \\ \nu_1 - \nu_1 e^{-\tau \frac{\theta_{2,1}}{\nu_1}} & \nu_2 + \nu_1 e^{-\tau \frac{\theta_{2,1}}{\nu_1}} \end{bmatrix} \quad (57)$$

the estimated transition is exact:  $\tilde{P}(\tau) \equiv P(\tau)$ .

**LBJf as Forward Euler.** In LBJf, we use the forward Euler approximation:

$$\tilde{P}_f^d(\tau) = P^d(0) + \tau \frac{d}{dt}P^d(t)|_{t=0} \quad (58)$$

The matrix form can be written as:

$$\tilde{P}_f(\tau) = \begin{bmatrix} 1 - \tau \sum_{j \neq 1} \theta_{1,j} & \tau \theta_{1,2} & \cdots & \tau \theta_{1,n} \\ \tau \theta_{2,1} & 1 - \tau \sum_{j \neq 2} \theta_{2,j} & \cdots & \tau \theta_{2,n} \\ \vdots & \vdots & \ddots & \vdots \\ \tau \theta_{n,1} & \tau \theta_{n,2} & \cdots & 1 - \tau \sum_{j \neq n} \theta_{n,j} \end{bmatrix} \quad (59)$$

One constraint we should take care of is that we need to restrict the simulation time  $\tau$  such that the diagonal of  $\tilde{P}_f$  is always non-negative.

**LBJb as Backward Euler.** In LBJb, we use the backward Euler approximation:

$$\tilde{P}_b^d(\tau) = P^d(0) + \tau \frac{d}{dt}P^d(t)|_{t=\tau} \Rightarrow \tilde{P}_b^d(\tau) = I + \tau \tilde{P}_b^d(\tau)Q^d \Rightarrow \tilde{P}_b^d(\tau) = (I - \tau Q^d)^{-1} \quad (60)$$

In general case, the matrix inverse does not have a closed-form solution and we use numerical method to solve the matrix inverse. As a result, when  $n$  is large, the LBJb is less efficient.

One thing need to notice is that  $(I - \tau Q^d)^{-1}$  gives a valid transition matrix. Firstly, all eigenvalues of  $Q^d$  are non-positive, hence  $I - \tau Q^d$  belongs to M-matrices and its inverse has all entries non-

negative Johnson & Smith (2011). Secondly, each row sum of  $I - \tau Q^d$  equals to 1, which means  $\mathbf{1} = (1, 1, \dots, 1)$  is an eigenvector with eigenvalue 1. Consequently,  $\mathbf{1}$  is also an eigenvector of  $(I - \tau Q^d)^{-1}$  with eigenvalue 1, which means that each row sum of  $(I - \tau Q^d)^{-1}$  is also 1.

## B.2 Complexity

In sampling, given the current state  $x$ , we first estimate  $\theta_{i,j}^d = g(\pi_{x^{d=j}} / \pi_{x^{d=i}})$ , where  $x^{d=j} = (x_1, \dots, x_{d-1}, e_j, x_{d+1}, \dots, x_D)$ . If we exactly evaluate the probability, it requires  $nD$  calls of the energy functions which is unaffordable except some special cases where the energy function has structures for fast evaluations of local change, e.g. Ising model, SK model. When the energy function is differentiable, a generic solution is estimating  $\theta_{i,j}^d$  through gradient (Grathwohl et al., 2021). In particular, we use the estimation:

$$\frac{\pi_{x^{d=j}}}{\pi_x} \approx \exp(-\langle \nabla f(x), x^{d=j} - x \rangle) \quad (61)$$

Given the current state  $x$ , we first evaluate the gradient  $\nabla f(x)$ , then the  $\theta_{i,j}^d$  can be easily estimated via inner-product. In this way, we only need to estimate the energy and the gradient twice for current state  $x$  and proposed new state  $y$  for each M-H step, which allows the proposal being scalable.

## C Experiment Details

We focus on discrete spaces of the form  $V = \mathcal{X}^D$  where  $\mathcal{X} = \{e_1, \dots, e_n\}$  is a finite set of one-hot vectors. We evaluate our methods on Bernoulli model, Ising model, factorial hidden Markov model and restricted Boltzmann machine. For each model, we consider both binary and categorical versions. For binary model, we use one smooth setting and one sharp setting. For categorical model, we use  $n = 4$  and  $n = 8$ . We report the detailed descriptions of the models and corresponding results in the following.

### C.1 Bernoulli Model

The Bernoulli distribution is the simplest distribution in a discrete space, where each site is independent with others. For  $x \in \mathcal{X}^D$ , the energy function is:

$$f(x) = \sum_{d=1}^D \langle x_d, \theta^d \rangle \quad (62)$$

where  $\theta^d \in \mathbb{R}^n$ . Across all settings, we use the entries in  $\theta_d$  independently sampled from centered normal distribution  $\mathcal{N}(0, \sigma^2)$ . For binary model we consider  $D = 10000$ . We use  $\sigma^2 = 0.125$  in the smooth setting and  $\sigma^2 = 12.5$  in the sharp setting. For categorical model, we consider  $D = 2000$ . We use  $\sigma^2 = 1.125$  for both  $n = 4$  and  $n = 8$ . The results are reported in Figure 3 and Figure 4. We can see that LBJ and LJB have substantial better efficiencies compared to other samplers. The weight function  $g(t) = \frac{t}{t+1}$  has better performance compared to  $g(t) = \sqrt{t}$  as proved in Zanella (2020). Moreover, the advantage of  $g(t) = \frac{t}{t+1}$  is more significant when the target distributions are sharper, which is consistent with the observation in continuous space

(Livingstone & Zanella, 2019).

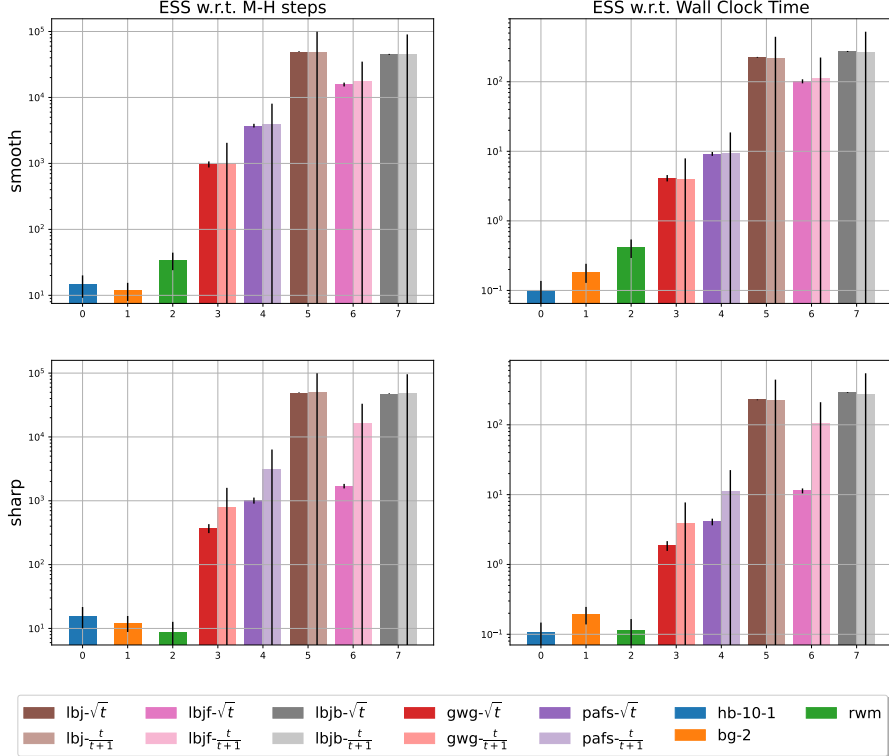


Figure 3: Evaluation on Bernoulli Models

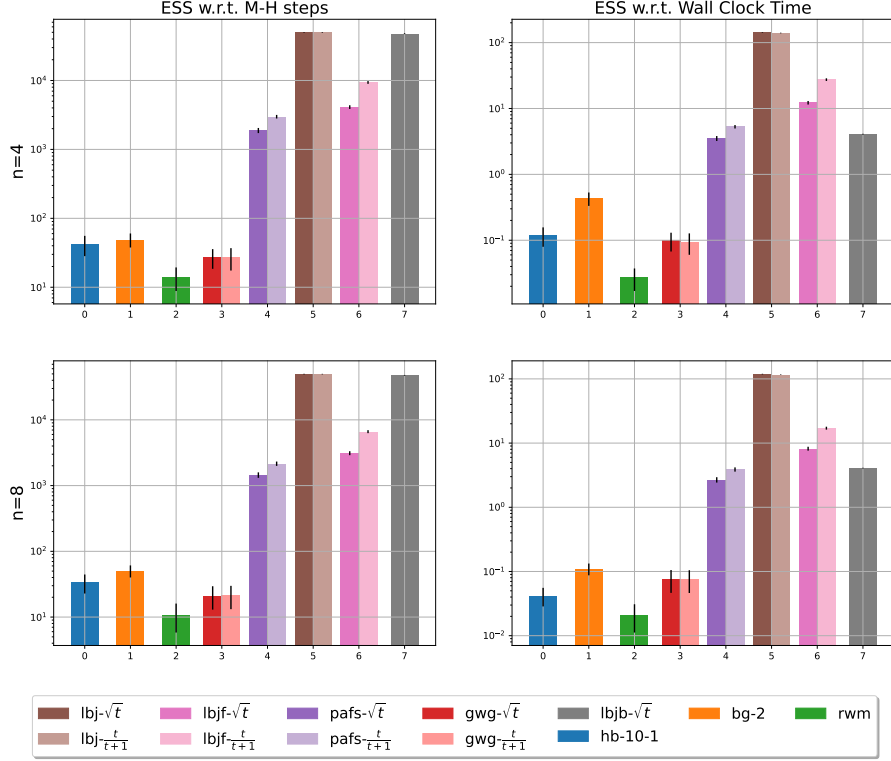


Figure 4: Evaluation on Categorical Models

## C.2 Ising Model

The Ising model (Cipra, 1987) is a mathematical model of ferromagnetism in statistical mechanics. It consists of binary random variables arranged in a lattice graph  $G = (V, E)$  and allows node to interact with its neighbors. The Potts model (Wu, 1982) is a generalization of the Ising model where the random variables are categorical. The energy function for Ising model and Potts model can be described as:

$$f(x) = - \sum_{d=1}^D \langle x_d, \theta^d \rangle - \lambda \sum_{(i,j) \in E} \delta(x_i, x_j) \quad (63)$$

where  $\theta^d \in \mathbb{R}^n$ ,  $\delta(x, y) = 1_{\{x=y\}}$ . For Ising model, we consider  $D = 2500$  where  $G$  is a  $50 \times 50$  square lattice, and we follow the settings in Zanella (2020). In smooth setting, we use  $\theta^d \sim \text{uniform}(-2, 1)$  for the outer part of the lattice graph, and  $\theta^d \sim \text{uniform}(-1, 2)$  for the inner part of the lattice graph. The connection strength is chosen as  $\lambda = 0.5$ . In sharp setting, we use  $\theta^d \sim \text{uniform}(-4, 2)$  for the outer part of the lattice graph, and  $\theta^d \sim \text{uniform}(-2, 4)$  for the inner part of the lattice graph. The connection strength is chosen as  $\lambda = 1.0$ . For potts model, we consider  $D = 900$  where  $G$  is a  $30 \times 30$  square lattice. For both  $n = 4, 8$ , we use entries in external field  $\theta_i^d \sim \text{uniform}(-1.5, 1.5) - 0.5 \frac{i}{n}$  for the outer part of the lattice graph, and  $\theta_i^d \sim \text{uniform}(-1.5, 1.5) + 0.5 \frac{i}{n}$  for the inner part of the lattice graph, where  $i = 1, \dots, n$ . The connection strength is chosen as  $\lambda = 1.0$ . The results are reported in Figure 5 and Figure 6. We can see that all LB samplers exhibit good performance. Among them, LBJ and LBJf are the most efficient. The weight functions  $g(t) = \sqrt{t}$  and  $g(t) = \frac{t}{1+t}$  each demonstrate advantages for different samplers.

## C.3 Factorial Hidden Markov Model

FHMM (Ghahramani & Jordan, 1995) uses latent variables to characterize time series data. In particular, it assumes the continuous data  $y \in \mathbb{R}^L$  is generated by hidden state  $x \in \mathcal{X}^{L \times K \times n}$ . The

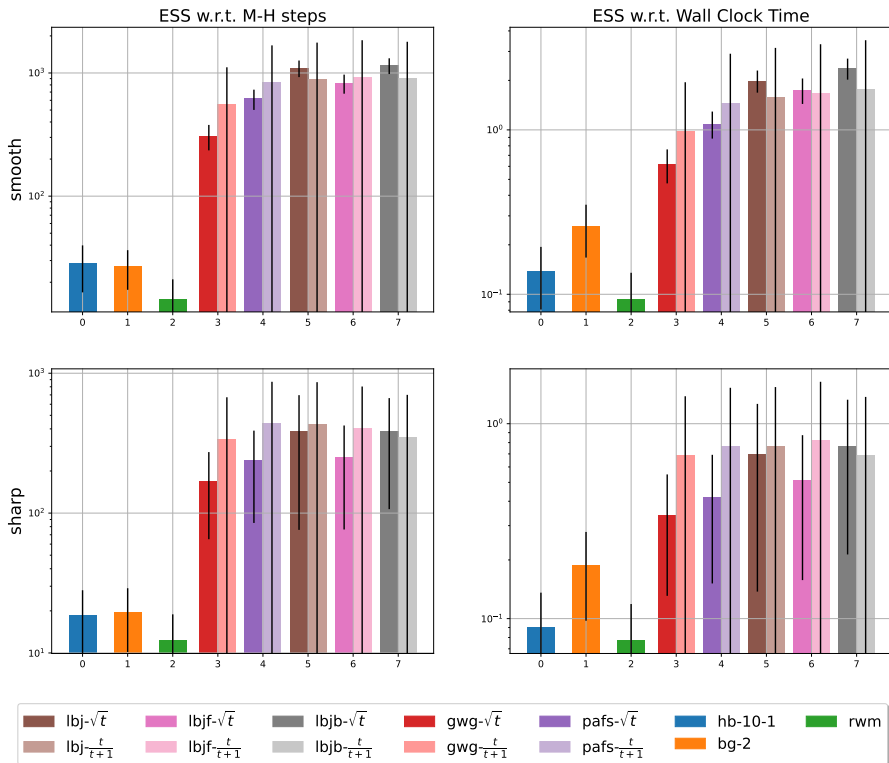


Figure 5: Evaluation on Ising Models

probability function is:

$$p(x) = p(x_1) \prod_{l=2}^L p(x_l | x_{l-1}), \quad p(y|x) = \prod_{l=1}^L \mathcal{N}(y_l; \sum_{k=1}^K \langle W_k, x_{l,k} \rangle + b; \sigma^2) \quad (64)$$

In particular, for binary model, we consider  $\mathbb{P}(x_1 = 0) = 0.9, \mathbb{P}(x_t = x_{t-1} | x_{t-1}) = 0.8, \sigma = 2.0$ . We use  $L = 1000, K = 10$  for smooth setting and  $L = 200, K = 50$  in sharp setting. For categorical model, we use  $p(x_1 | x_1 \neq 0)$  and  $p(x_t | x_{t-1}, x_t \neq x_{t-1})$  as uniform distribution and we use  $L = 200, K = 10$ . We report the results in Figure 7 and Figure 8. Similar to the Ising model, we can see that all locally balanced samplers demonstrate good performance. In FHMM, PAFS has an efficiency very close to the LBJ samplers. We believe this is because the energy change rate is stable in FHMM and the magnitude of the gradient changes steadily. Hence the Hamming distance works as a good metric. We also note that the weight function  $g(t) = \sqrt{t}$  is systematically better than  $g(t) = \frac{t}{t+1}$  on FHMM. This is consistent with the observation in Livingstone & Zanella (2019) that  $g(t) = \sqrt{t}$  performs better on smooth target distributions and  $g(t) = \frac{t}{t+1}$  performs better on nonsmooth target distributions, although Livingstone & Zanella (2019) focus on the sampling in continuous spaces.

#### C.4 Restricted Boltzmann Machine

The RBM is an unnormalized latent variable model, with a visible random variable  $v \in \mathcal{X}^D$  and a hidden random variable  $h \in \{0, 1\}^M$ . When  $v$  is binary, we call it a binary RBM (binRBM) and when  $v$  is categorical, we call it a categorical RBM (catRBM). The energy function of both binRBM and catRBM (Tran et al., 2011) can be written as:

$$f(v, h) = - \sum_{d=1}^D \langle v_d, \theta_d \rangle - \sum_{m=1}^M \beta_m h_m - \sum_{d,m} \langle h_m \theta_{m,d}, v_d \rangle \quad (65)$$

Unlike the previous three models, where the parameters are hand designed, we train binary RBM on MNIST (LeCun et al., 1998) and categorical RBM on Fashion-MNIST (Xiao et al., 2017) using contrastive divergence Hinton (2002). Across all settings, we have  $D = 784$ . For binary models,

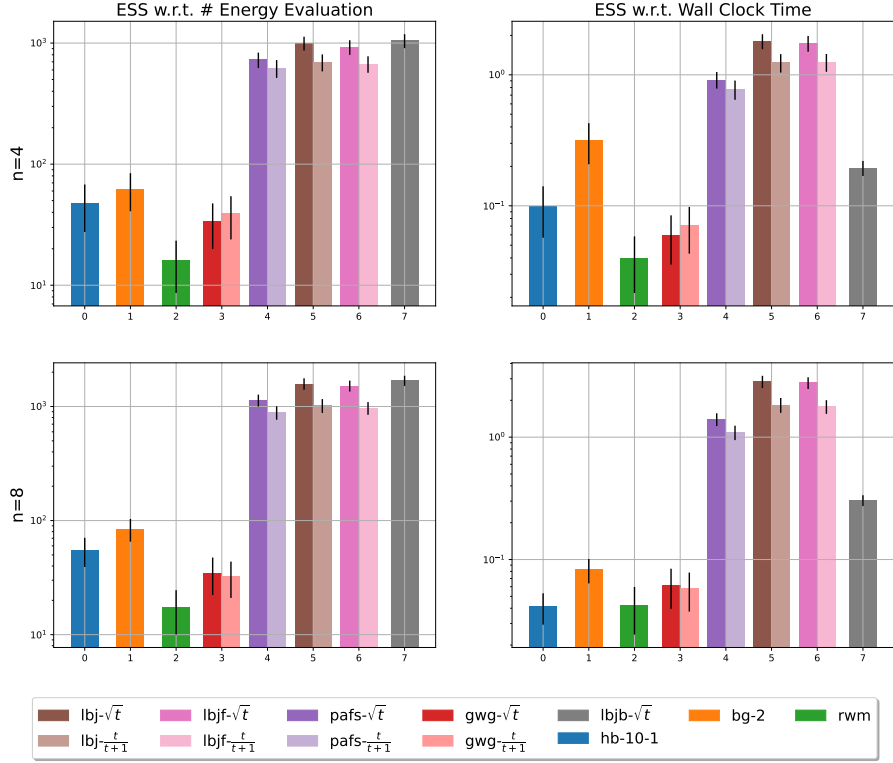


Figure 6: Evaluation on Potts Models

we use  $M = 25$  for smooth setting and  $M = 500$  for sharp setting. For categorical models, we use  $M = 100$ . We report the results in Figure 9 and Figure 10. The learned RBMs have stronger multi-modality compared to previous models. We can see that, as before, LBJ and LJB lead in proposal quality, while LBJ is the most efficient overall.

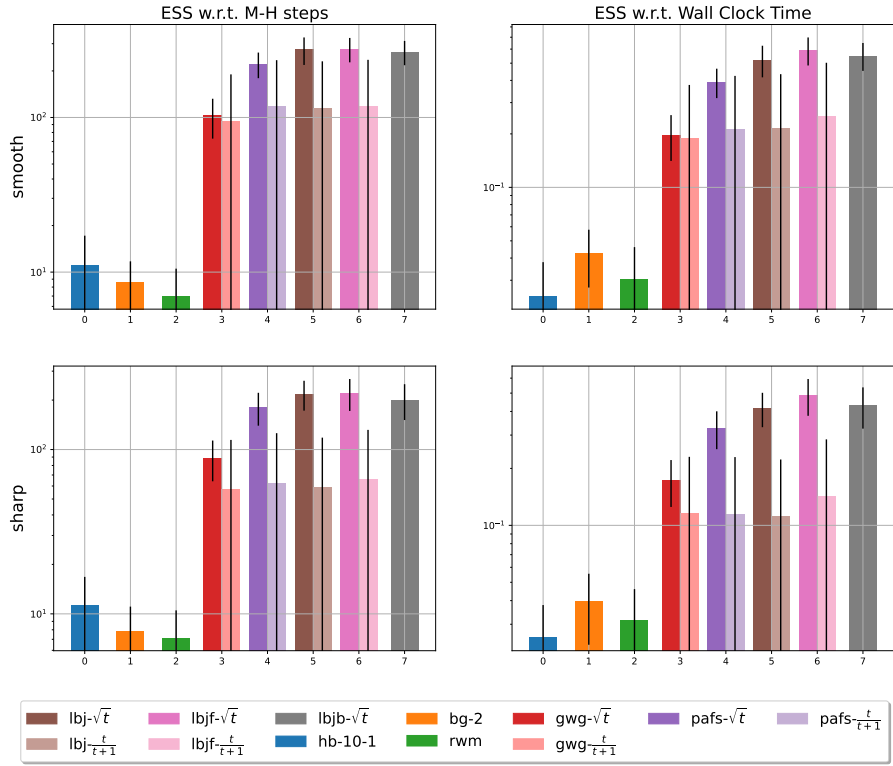


Figure 7: Evaluation on binFHMM

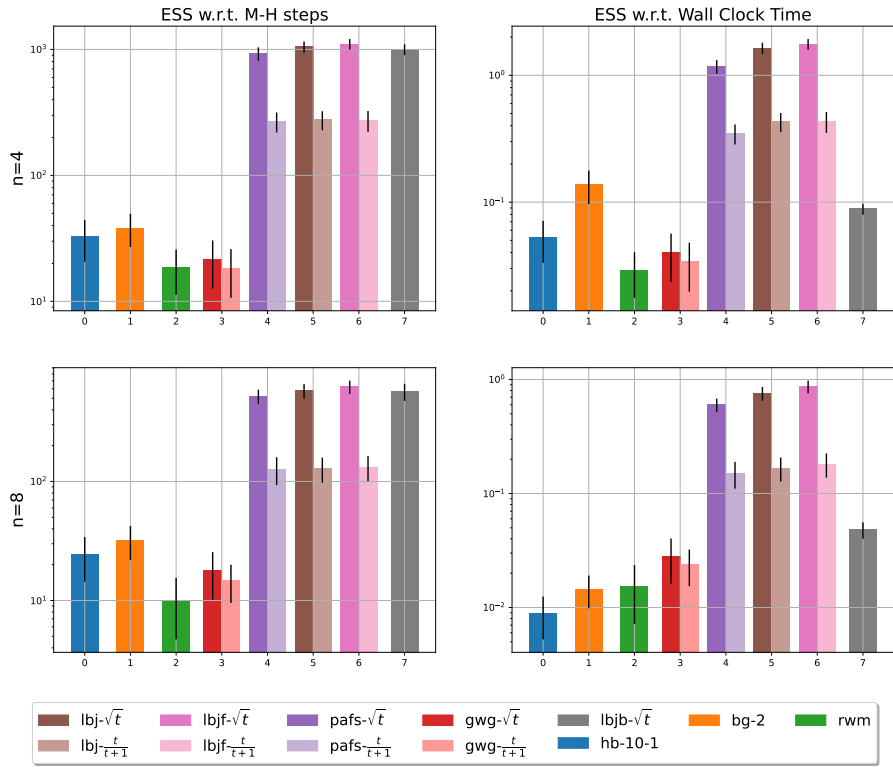


Figure 8: Evaluation on catFHMM

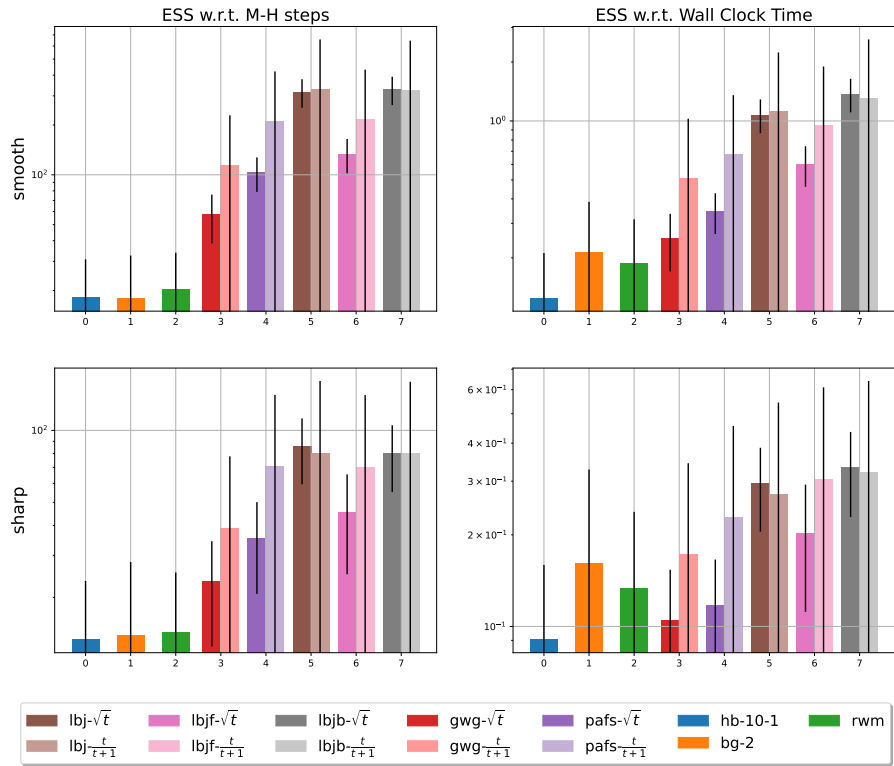


Figure 9: Evaluation on binRBM

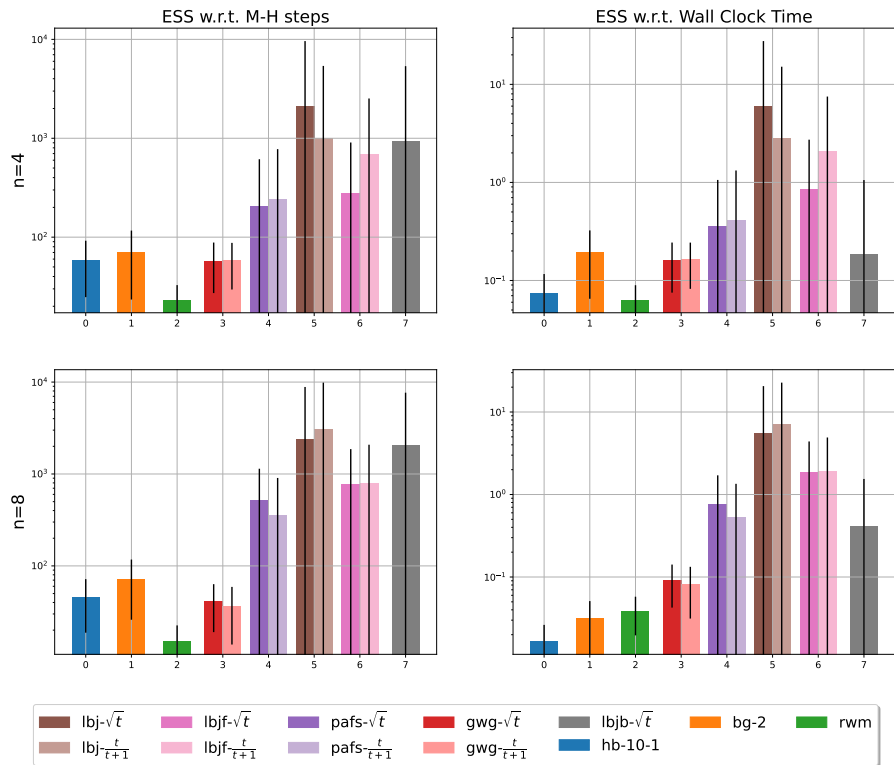


Figure 10: Evaluation on catRBM